Hidden soils and their carbon stocks at high-elevation in the European Alps (North-West Italy)

Published version:

DOI:10.1016/j.catena.2020.105044

Hidden soils and their carbon stocks at high-elevation in the European Alps (North-West Italy)

Emanuele Pintaldi[1], Michele E. D'Amico[1*], Nicola Colombo[1,2,3], Chiara Colombero[4], Luigi Sambuelli[4], Claudio De Regibus[4], Diego Franco[4], Luigi Perotti[3], Luca Paro[5], Michele Freppaz[1,2]

[1]University of Turin, Department of Agricultural, Forest and Food Sciences (DISAFA), Largo Braccini, 2, 10095 Grugliasco (TO), Italy.

[2]University of Turin, Research Center on Natural Risk in Mountain and Hilly Environments (NatRisk), Largo Braccini, 2, 10095 Grugliasco (TO), Italy.

[3]University of Turin, Department of Earth Sciences (DST), Via Valperga Caluso, 35, 10125 Turin, Italy.

[4]Politecnico di Torino, Department of Environment, Land and Infrastructure Engineering (DIATI), Corso Duca degli Abruzzi, 24, 10129 Turin, Italy.

[5]Regional Agency for Environmental Protection (Agenzia Regionale per la Protezione Ambientale - ARPA) of Piedmont, Via Pio VII, 9, 10135 Turin, Italy.

Abstract

Alpine soils store large quantities of total organic carbon (TOC). Given their high sensitivity to climate change, they may release large amounts of CO_2 in a warming climate scenario. Thus, it is important to know their C stocks in order to estimate its possible release. While C stocks of forest, dwarf shrub and alpine grassland soils are well documented, little is known about soils and C stocks in high-elevated periglacial environments dominated by frost-driven processes. The object of this study is the periglacial environment of the Stolenberg Plateau (LTER site Istituto Mosso, 3030 m a.s.l.), at the foot of the Monte Rosa Massif (NW Italian Alps). The plateau is mostly covered by a thick stony layer, organized in periglacial blockfields and blockstreams. The plant cover reaches only 3-5%. During the construction of a chair lift, open trenches revealed, unexpectedly, well-developed soils under the active periglacial stone cover. In particular, thick (30-65 cm) and dark TOC-rich A horizons were observed. Below these Umbric horizons, Cambic Bw ones were developed but discontinuous. Despite the lack of vegetation, C stocks were remarkably high (up to ~5 kg m^{-2}), comparable to vegetated soils at lower elevation. Non-invasive geophysical methods revealed that these hidden soils were widespread on the plateau under the stony cover, with a mean thickness of around 50 cm. These TOC-rich soils, without vegetation and covered by periglacial landforms, represent a unique pedoenvironment suggesting new perspectives on the actual C-stocks at high-elevation sites, which are probably underestimated.

Keywords

Soil organic matter; Periglacial; Blockstream/Blockfield; Skeletic Umbrisol (Arenic, Turbic)

1 Introduction

Soil Organic Matter (SOM) stored in alpine soils (i.e. soils developed above the timberline, in alpine tundra and alpine desert, etc.) represents a considerable part of the global C cycle (e.g. Bockheim and Munroe, 2014), acting as a sink for carbon dioxide and having therefore a great potential to sequestrate this from the atmosphere (Bojko and Kabala, 2017). Alpine soils, especially those covered by vegetation and/or affected by permafrost, store large quantities of organic carbon (e.g. Celi et al., 2010; Bockheim and Munroe, 2014). However, given the high sensitivity of soils to climate change (Hagedorn et al., 2010a; Stanchi et al., 2015), they may release large amounts of carbon dioxide in a warming climate scenario (e.g. Hagedorn et al., 2010b; Schuur et al., 2013; Knowles et al., 2019). Generally, at high elevations in the European Alps, soils are mainly classified as Regosols, Cambisols, or Podzols (e.g. Egli et al., 2006; Zollinger et al., 2013; D'Amico et al., 2020), often showing evidences of cryoturbation. In particular, high-elevation soils (i.e. above the alpine treeline) are affected by frost-action processes (e.g. frost-shattering, frost sorting, frost heave, solifluction etc.) (Karte, 1983), induced by seasonal frost penetration and/or permafrost (Van Vliet-Lanoë, 2014), leading to the formation of patterned ground, typical of periglacial environments (e.g. tilting of stones, blockstreams, blockfields, wedges, etc.) (e.g. Goodfellow, 2007; D'Amico et al., 2019). As these processes are mostly driven by temperature, active patterned ground is sensitive to climate warming, which can induce several effects such as permafrost degradation (e.g. Biskaborn et al., 2019; Mollaret et al., 2019), expansion of plant cover (e.g. Gerdol and Smiraglia, 1990), transition from pioneer species communities towards more acidophilous grassland (D'Amico et al., 2015), and increased SOM decomposition (e.g. Arteaga et al., 2008; Hagedorn et al., 2010a).

While the carbon stocks of forest and alpine grassland soils are well documented by several studies (e.g. Leifeld et al., 2009; Zollinger et al., 2013; Bockheim and Munroe, 2014), very little is known about carbon stocks in high-elevated periglacial environments, especially in the European Alps. This is probably due to different reasons, such as: 1) these soils are located in very unfavorable positions at high elevation and they are often difficult to reach, requiring specific technical equipment; 2) generally, these high-elevation areas are not covered by vegetation, therefore, as plants are the primary carbon source, these soils received less interest since they are not considered a relevant carbon sink compared to other soils; 3) high-elevation soils are often in periglacial environments, which are characterized by cryoturbation processes (induced by low temperatures and/or permafrost) that allow the formation of patterned ground and solifluction, which create an extreme spatial variability (D'Amico et al., 2015). They are frequently covered by coarse debris which makes it difficult to recognize them as soils and perform in-depth pedological investigations using manual devices.

In order to deepen the knowledge on these periglacial stone-covered environments, geophysical methods can be used thanks to their capability to map soil thickness even in areas with undulating topography, complex spatial distribution and non-homogeneous or anisotropic properties of the investigated materials. Among the available geophysical methods, Electrical Resistivity Tomography (ERT) allows investigating contrasts in electrical properties between the soil (loose, porous, prone to water retention and possibly rich in organic matter) and massive bedrock or coarse deposits. The same contrast in physical properties, together with differences in layering and other internal structures, can be imaged using Ground Penetrating Radar (GPR) profiling. ERT and GPR are widely used to support pedological surveys for soil characterization, mapping of the presence, depth and lateral variability of soil horizons, agricultural purposes and contamination analyses from low to mid latitudes and elevations (e.g. Samouelian et al., 2005; Allred et al., 2008; Doolittle and Butnor, 2009; Andre et al., 2012; Nováková et al., 2013). By contrast, only few applications of geophysical prospections for the study of high-elevation soils are reported in the literature (e.g. Leopold et al., 2010; Pellet et al., 2016; Mollaret et al., 2019). In periglacial environments, these techniques are mainly used for permafrost characterization, hydrogeological processes and loose material-bedrock interface recognition (Moorman et al., 2003; Otto and Sass, 2006; Kneisel et al., 2008; McClymont et al., 2010; Léger et al., 2017).

The research was performed in the severe periglacial environment of the Stolenberg Plateau on the southern slope of Monte Rosa Massif (NW Italian Alps) where, in 2017, unexpected well-developed soils within blockfields/blockstreams were found. Considering the impossibility to deepen the investigation using manual devices and machinery, and the necessity to detect the distribution of these hidden soils, non-invasive geophysical methods were applied in September 2019.

In this context, this work aims at: 1) describing and classifying the hidden soils, 2) determining their carbon stock, and 3) investigating their local distribution and thickness, and potential relationships with permafrost presence/distribution.

2 Materials and methods

2.1 Study Area

The work was carried out in the periglacial environment of the Stolenberg Plateau, a 13,500 m^2 almost flat area located at 3030 m a.s.l., at the boundary between Valle d’Aosta and Piemonte regions (Fig. 1a), at the foot of the southern slope of Monte Rosa (4634 m) (NW Italian Alps). The study site represents the summit portion of the Long Term Ecological Research (LTER) site Angelo Mosso Scientific Institute (LTER-Italia IT19-001-T), belonging to the LTER-Italy network. The study area is also a Site of Community Importance and a Special Protection Area (SCI/SPA IT1204220 “Ambienti glaciali del gruppo del Monte Rosa”) (European Commission, 1992) belonging to the Natura 2000 network.

From 2007 to 2018, the area had a mean annual air temperature of –2.2 °C, a mean cumulative annual snowfall of 818 cm, and a mean annual liquid precipitation of ca. 400 mm. Snow cover lasts for at least 8 months, reaching a maximum thickness of ca. 350 cm (Freppaz et al., 2019). In the LTER-Italia IT19-001-T site, although at lower elevation and with alpine vegetation cover (snowbed and grassland communities), soils were classified as Skeletic Dystric Regosol, Skeletic Umbrisol, and Skeletic Dystric Cambisol (IUSS Working Group WRB, 2015) (Magnani et al., 2017). Permafrost was detected at depths higher than 3-4 m on the nearby Corno del Camoscio (3024 m a.s.l.) (Colombo et al., 2019). On the plateau, the slope steepness is below 10%, with large flat portions in the central and eastern parts. The area shows typical features of periglacial environments, characterized by active periglacial landforms. In particular, the plateau is covered by a thick layer of stones with variable size (from decimeter to meter), well organized in blockfields, blockstreams/sorted stripes, gelifluction lobes, tilted stones and weakly developed sorted circles (Fig. 1b). In particular, blockstreams partly rearranged into sorted stripes are visible on sloping surfaces, while blockfields, partly rearranged into patterned ground and rich in standing stones, dominate the flatter surfaces. The activity of the periglacial processes is evidenced by the absence of lichens from most stones (Ballantyne and Matthews, 1982). The parent material is composed of gneiss and mica-schists (Monte Rosa nappe, Pennidic basement) and metabasites (Zermatt-Saas unit) (Mattirolo et al., 1951). No traces of glacial till are observed, as all blocks seem autochthonous

(Ballantyne, 2010; Goodfellow, 2007); the best developed blockstreams are located around rock outcrops, and are clearly derived by their cryofracturation. The glacial history of the plateau is currently unknown.

The vegetation cover, which is extremely scarce and confined to small patches reaching no more than 5% of the plateau areal extension, is composed mainly of alpine and nival species such as *Silene acaulis*, *Carex curvula, Salix herbacea* in the vegetated patches, while *Festuca halleri*, *Poa alpina*, *Ranunculus glacialis*, *Leuchantemopsis alpina*, *Cerastium uniflorum* and a few other pioneer species grow also in the stone-covered area, with extremely low cover values. A higher vegetation cover characterizes a small area in the northern side, close to the edge of the cliff, on slightly more weatherable amphibolites.

2.2 Soil survey, sampling and analysis

In 2017, during the operational activities for the construction of a new chair lift, the largest part of the plateau was delimited in order to protect the natural environment (Directive, 1992) and the periglacial features against the excavation operations. However, three trenches were opened (2 to 10 m long, to a depth of around 1.2 m) in the construction area, revealing unexpected, well-developed soils under the stony cover. This finding was possible only thanks to the machinery employed, whose utilization was exceptionally allowed for the construction of the chair lift station.

Field description of soil transects was performed according to FAO (2006), while soil classification was done according to WRB classification system (IUSS Working Group WRB, 2015). The three trenches (soil profiles) were described and sampled (Fig. 1a). Each profile was subdivided into sectors characterized by a similar sequence of horizons. Overall, 27 soil samples were collected from all genetic horizons in the profiles; at least one sample per genetic horizon was sampled in each sector (ca. 300-500 g per sample). The samples were air-dried, sieved to 2 mm and analyzed following the standard methods reported by Van Reeuwijk (2002). The pH was measured in soil-water suspension (soil:water = 1:2.5). The particle-size analysis was performed by the pipette method after organic matter destruction with H_2O_2 followed by dispersion with Na-hexametaphosphate. Total carbon (corresponding to total organic carbon-TOC due to the absence of carbonates) and nitrogen (TN) concentrations, were measured by dry combustion with an elemental analyzer (CE Instruments NA2100, Rodano, Italy).

The soil organic carbon stock (C-STOCK$_{tot}$ kg m^{-2}) of the profiles was calculated for sectors in which the horizons sequence was similar, according to the following equation adapted from Batjes (1996):

$$C - STOCKtot = \sum_{i=1}^{n} \frac{\mathrm{TOC} * \mathrm{BD} * \mathrm{TH} * \mathrm{VF}}{1000} \qquad (1)$$

where *n* is the number of soil horizons of each sector, TOC is the soil organic carbon concentration (g kg^{-1}) of the mineral horizons, BD is the Bulk Density (kg m^{-3}) based on mean Bulk Density values of high-elevation soils (D'Amico et al., still unpublished) measured according to Boone et al. (1999), TH is the horizon thickness (m), VF is the volume of fine earth excluding the coarse mineral fraction (> 2 mm, visually estimated in the field (%) for each horizons), calculated as [1 – (% rock volume/100)], 1000 is the unit correction factor.

In order to support the interpretation of the geophysical measurements, the clay minerals were analyzed using a Philips PW1710 X-ray diffractometer (40kV and 20 mA, CoKα radiation, graphite monochromator). The Mg saturated clay fraction (< 2 µm) was separated by sedimentation, flocculated with $MgCl_2$, washed until free of Cl$^-$, and freeze-dried. Scans were made from 3 to 35 °2θ at a speed of 1 °2θ min^{-1}, on air dried, ethylene glycol solvated, and heated (350° and 550 °C) oriented mounts. A semi-quantitative evaluation of mineral abundance was performed using the Mineral Intensity Factors method (Islam and Lotse, 1986), which considers peak areas. For the calculation, the background was subtracted and the peak positions, intensities and areas were calculated using the PowderX software (Dong, 1999).

2.3 Geophysical investigation

Six 48-electrode Electrical Resistivity Tomography (ERT) profiles were acquired (Fig. 1a). Five of them had an inter-electrode spacing of 0.30 m, for a total length of 14.1 m. One longer profile (ERT 3 in Fig. 1a) was acquired with a spacing of 2 m between the electrodes, for a total length of 94 m. With the short profiles we aimed at the detection and lateral imaging at shallow depths of the buried soils with high-resolution, while the longer line was designed for a deeper general low-resolution characterization of the bedrock conditions below the soil horizons. To constrain data interpretation, reference values for the soil electrical resistivity were derived from the statistical analysis of measurements carried out in an uncovered soil outcrop (approximately 1.5 x 0.3 m) with a single quadrupole (0.25-, 0.30- and 0.40-m electrode spacing, eight array configurations of current and potential electrode positions).

ERT electrodes were georeferenced using a Garmin GPS 60 system to overlay the position of each survey line on a high-resolution digital surface model (DSM) of the plateau and later account for the significant topographic variations in the inversion of the longest ERT line. Digital vertical and slantwise photos obtained from an Unmanned Aerial Vehicle (UAV) survey were processed with structure from motion and multi-view-stereo algorithms to produce a high-resolution DSM (10 cm / pixel ground resolution) of the investigated area (e.g. Smith et al., 2015; Carrivick et al., 2016, Alberto et al., 2018) (Supplementary Material, SM1).

Ten ground penetrating radar (GPR) profiles (Fig. 1a) were complementary acquired with a 500-MHz antenna controlled by an IDS K2 digital acquisition unit. GPR traces were acquired for a total time of 100 ns and 512 samples per trace. Ublox EVK-5T GPS was used to track each survey position. The average distance between subsequent traces resulted in 0.025 m along each line.

Local rare diffraction hyperbola in the processed radargrams were fitted with a velocity of 0.1 m/ns. To apply this value for time-to-depth conversion, the medium velocity (v) was additionally estimated by the Complex Refractive Index Method (CRIM, Birchak et al., 1974; Wharton et al., 1980), following:

$$\sqrt{\varepsilon_S} = (1-\varphi)\sqrt{\varepsilon_m} + \varphi\, S\sqrt{\varepsilon_w} + \varphi\,(1-S)\sqrt{\varepsilon_a} \qquad (2)$$

and

$$v = \frac{c}{\sqrt{\varepsilon_S}} \tag{3}$$

where $\mathcal{E}_S$, $\mathcal{E}_m$, $\mathcal{E}_w$ and $\mathcal{E}_a$ are the relative dielectric permittivities of soil (solid matrix + pore space), solid matrix, pore water and air respectively, φ is the soil porosity, S is the degree of water saturation and c is the electromagnetic wave velocity in vacuum ($3 \cdot 10^8$ m/s). In Equation 2, $\mathcal{E}_a=1$, $\mathcal{E}_w=77.8$ (from GPR measurements on the water of a nearby pond; Colombo et al., 2018) and $\mathcal{E}_m=7$ (from average reference values of similar loamy sandy soils, e.g. Daniels, 2004). Soil porosity φ was indirectly estimated from density measurements in the range 0.5 to 0.6. Moist (unsaturated) conditions were present on site during GPR acquisitions. A variable S, between 0.2 and 0.4, was consequently considered in the computation. Using these parameters, average $\mathcal{E}_S=9.3$ and v=0.10 m/ns were obtained for time-to-depth conversion. The approximate wavelength of a 500-MHz GPR signal in this material is consequently 0.2 m, meaning approximately 0.1 m of vertical resolution (half wavelength) in the investigated medium.

Additional details on ERT and GPR processing are given in Supplementary Material SM2.

2.4. Bottom temperature of snow cover and ground temperature

To investigate the ground surface thermal conditions in the investigated area, the bottom temperature of the snow cover (BTS, e.g. Hoelzle, 1992) measurements were performed in 2014, 2015, and 2019. To acquire BTS data, a thermometer Delta Ohm RTD HD 2307.0 (accuracy ±0.05 °C, resolution 0.1 °C), equipped with a probe Pt100 TP474C.0, was installed on a stainless steel probe. The location of each sample point was recorded with a handheld Global Positioning System (GPS) ("Aventura" TwoNav vs. 2.6.2). The measurements were performed during the late winter (March/April), when a sufficient snow cover was established since at least one month, before the onset of snow melt. Since a minimum snow thickness of 80 cm is necessary to provide a sufficient insulation against air temperature variations, measurements were made only where this threshold was found, obtaining about 260 measurements.

Ground temperature (GT) data from a 5-m deep borehole managed by Arpa Piemonte in the north-eastern side of the plateau were also used to analyse the ground thermal conditions. Daily data from 04 November 2017 to 29 July 2019 were analysed; no data gaps were present in the series.

3 Results

3.1. Soil profiles characteristics

The stony/blocky layer (blockfields and blockstreams, respectively on flat surfaces or on gentle slopes) was 10-60 cm thick, and it was usually well graded with depth, with the coarsest stones on the surface and fine ones at the bottom, associated with A1 horizons, as typically observed in blockfields and blockstreams (Wilson, 2013). Below the stone layer, the profiles were characterized by thick (between 30 and 65 cm) and continuous, dark A and A@ horizons with subangular-blocky, platy or granular structure (Table 1, Figs. 2, 3 and 4). These horizons were characterized by few living or dead roots and very few, extremely weak, isolated, biogenic fine granular aggregates. They were classified as Umbric horizons according to WRB (IUSS Working Group WRB, 2015). In fact, the diagnostic criteria for Umbric horizons, calculated in the top 20 cm, are dark colors (moist chroma and value ≤3), darker colors than the horizons underlying it or the parent material, soft or friable consistence and not massive structure, ≥ 0.6% TOC, pH < 5.5 or base status < 50%. Below the Umbric horizons, Cambic Bw ones were often developed although discontinuous, characterized by brown color and well-developed subangular-blocky structure (Table 1, Figs. 2, 3 and 4). Stones were quite scarce, particularly in A horizons, evidencing frost sorting and cryoexpulsion. The stones were moderately weathered and were quite easily broken with a spade, particularly in Bw horizons, while they were weakly weathered in the surface layer. Cryoturbation features, such as inclusions of surface A materials at depth (horizons n. 7 in Fig. 3) as well as convolutions and block displacement above wedges, were often observed within the profiles. In profile 3, blocks shown as “a” in Fig. 2 were dislocated and raised by freeze-thaw processes from the rock layer evidenced by letters “b” and “c”, above a deep fracture (wedge). Thick, dense silt caps were also observed on the upper faces of stone fragments. Below the Bw, BC and CB horizons, the highly fractured bedrock was always observed. The soils were classified as Skeletic Umbrisol (Arenic, Turbic), according to IUSS Working Group WRB (2015).

3.2 Soils physical and chemical properties

The soil texture of all horizons was generally loamy sand or sandy loam, with a substantial prevalence of sand (77% on average) compared to silt (20%) and clay (3%) fractions (Tab. 1). The clay fraction was composed of ca. 60% quartz, 20% mica/illite, 10% chlorite, 10% plagioclase and other minerals in traces (not shown), reflecting a similar mineralogy as the parent material. pH values were extremely to moderately acidic, ranging between 4.3 and 5.9. TOC content spanned from 0 to over 2%, reaching maximum values in A horizons, while TN values were very low in all the samples. The TOC/TN ratio ranged between 7 and 20, reaching maximum values in the A horizons.

Considering the overall C-STOCK$_{tot}$ of each sector within the profiles (Table 2, Figs. 2, 3 and 4), in P1 the values ranged between 0.7 and over 5 kg m^{-2}, reaching minimum and maximum values in sector C and A respectively; in the profile P2 the values spanned from 1.12 to approx. 3 kg m^{-2} reaching minimum values in sector D and maximum in sector F; the C-STOCK$_{tot}$ of P3 reached the minimum value of 2.17 kg m^{-2} in sector K and a maximum of 3.30 in kg m^{-2} in the sector I.

3.3 Geophysical investigation

Results obtained from the long ERT line (ERT3 in Fig. 5a) provided a non-homogeneous electrical resistivity distribution in the plateau bedrock. The deepest values (6-8 kΩ m in the line center below

5-m depth, yellow in Fig. 5a) were interpreted as representative of compact bedrock. Higher resistivities (>8 kΩ m, green in Fig. 5a) were depicted at shallower depths, reaching values of 50 kΩ m in proximity of the fractured overhanging rock cliff delimiting the plateau eastern edge. These values were related to variable fracturing conditions of the shallow bedrock, increasing towards E and NE. An isolated high-resistivity area (> 75 kΩ m) was found at approx. 2 m depth towards the E-NE section of the ERT3 (Fig. 5a).

Above the fractured bedrock, all the short ERT lines revealed the presence of a distinct and discontinuous layer with variable thickness under the stony cover, with resistivity values lower than 6 kΩ m (orange to red in Fig. 5, b to d). Separated measurements acquired on an uncovered soil outcrop showed resistivity values in the range 2.9-4.2 kΩ m, with an average of 3.6 kΩ m over 24 tests with different array spacing and electrode configuration. Consequently, this shallow layer was interpreted as representative of the soil presence under the periglacial cover.

The GPR profiles depicted a complex stratigraphy in the first meters of depth. Exemplificative results are illustrated in Fig. 6 for the GPR profiles acquired along the ERT lines of Fig. 5. Processed radargrams were visually interpreted as shown in Fig. 6a. In the shallowest part of each section, GPR reflections appear as laterally continuous, smooth and sub-horizontal, likely due to the soil presence (s in Fig. 6a). Below this layer, intricate patterns of discontinuous GPR reflections are conversely present, more steeply dipping in different directions. This layer (t in Fig. 6a) possibly corresponds to the transition between soil and bedrock. The chaotic arrangement of soil material and debris resulting from the fractured bedrock may have generated this complex GPR response. At depths higher than 1 m, GPR reflections show again a more homogeneous lateral continuity, possibly indicating the bedrock presence (b in Fig. 6a).

Given the difficulty and subjectivity in manually picking the soil bottom basis from GPR sections (Fig. 6, b, d and f), ERT results (Fig. 5) were transformed in total gradient sections of electrical resistivities. The gradient maxima in each section were then automatically picked and interpreted as objective markers of the presence of a sharp vertical and lateral contrast between soil and surrounding materials and consequently used to estimate the average soil thickness in the plateau. Results are shown in Fig. 6 (c, e and g) in comparison with manual picking performed on GPR sections. Electrical resistivity gradient maxima generally fall within the transition layer (Fig. 6a) depicted in GPR results, providing a rough estimate of the soil-substrate interface.

The soil presence was detected by both geophysical methods within the first meter of depth of all the investigated lines.

3.4 Ground temperature conditions (BTS and GT)

The BTS measurements highlighted a thermal difference between the northern and the southern side of the plateau. Colder ground surface temperatures (often below -2/-3 °C) in the southern portion of the plateau gradually became warmer (generally above -2/-1 °C) towards the northern zone, where only few spots highlighted temperature below -2/-3 °C (Fig. 7a). In additions, a clear correspondence between a cold BTS spot and a high resistivity body detected by the long ERT3 was found (Fig. 7a). Regarding the borehole, maximum GTs reached decisively positive values at all depths during the investigated period (Fig. 7b).

4 Discussion

4.1 Soil properties and carbon stocks

The opening of trenches revealed the unexpected presence of complex and well-developed soils (Umbrisols) under the stony cover, with convolutions and inclusions of different materials, as a result of intense cryoturbation processes as described by Bockheim and Tarnocai (1998) in permafrost-affected soils. Despite the strong geomorphic activity characterizing this periglacial area, the observed soils were extremely well developed, particularly inside periglacial landforms (blockfields and blockstreams). Considering the remarkable thickness of A horizons (up to 60 cm), these soils are considerably more developed than the surrounding soils with or without vegetation, at similar or lower elevation, where weakly developed and shallow Skeletic Regosols, Cambisols or Umbrisols (e.g. Magnani et al., 2017) with thinner A horizon (up to 25-30 cm) were common. Nevertheless, the textural class as well as the pH values were comparable to those found in the surrounding soils under snowbed vegetation (e.g. Magnani et al., 2017). In the Italian Alps, very few works reported soils with C-rich A horizons at high elevation (around 3000 m a.s.l.), for instance Baroni and Orombelli (1996) describe Inceptisols with C-rich A horizons at the Tisa Pass (~ 3200 m a.s.l, Eastern Alps, close to the Italian-Austrian border), although thinner and less developed compared to our soils.

Considering the absence of a significant vegetation cover on the plateau and the high elevation, the estimated total carbon stock for each sector was surprisingly high. Overall, the carbon stocks were comparable to the ones reported for high-elevation, cryoturbated soils in the Aosta Valley, although generally covered by alpine tundra, for which values around 2-3 kg m^{-2} (D’Amico et al., still unpublished) were calculated. The values were also in the range reported for other vegetated soils in Alpine tundra ecosystems (Bockheim and Munroe, 2014). Moreover, our results, in particular from soil profile P1, despite the lack of vegetation, were also in the normal range of carbon stock values from moderately developed forest or heath soils in the Aosta Valley, such as Entic Podzols (D’Amico et al., 2020), and to those reported by Chiti et al. (2012) for forest ecosystems in Spain, for mountain boreal forests in North America (Hoffmann et al., 2014) or for mountain soils in the Veneto region (North-East Italian Alps) (Garlato et al., 2009).

4.2 Soil distribution, depth and subsurface morphology of the plateau

Geophysical investigations confirmed the widespread presence of soils on the whole plateau. Considering the soil texture, the measured electrical resistivity values (up to 6 kΩ m) may appear unusually high for field tests carried out in moist (but unsaturated) conditions on these materials. Since the proportion of minerals having relevant surface conductivity was found to be almost negligible (i.e. illite and chlorite are less than 1% of the total solid matrix), a rough check on the expected soil electrical resistivity ρ_S can be performed following Archie's law (Archie, 1942):

$$\rho_S = a\,\frac{\rho_w}{\varphi^m S^k} \tag{4}$$

where ρ_w is pore water resistivity (around 100 Ω m, i.e. moisture mainly due to precipitation and shallow seepage), a=1 and m=1.4 are Archie's coefficients for non-consolidated sediments (Archie, 1942; Friedman, 2005), φ is the soil porosity (0.5 to 0.6), S is the degree of water saturation and k coefficient can be assumed equal to 2 for S>0.1. Applying Equation 4, retrieved ρ_S values are in the range 1.3-6.5 kΩ m for S between 0.2 and 0.4, thus additionally confirming the obtained electrical resistivity values.

Thanks to the electrical resistivity gradient maxima analyses, the soil-substrate interface was recognized at depths ranging from 26 to 88 cm, for an average of 47 cm over the five short ERT lines. In general, higher depths (and soil thicknesses) were identified in the eastern part of the plateau (ERT2, ERT5 in Fig. 1a), close to the chair lift station, in presence of a more fractured underlying bedrock and below a particularly coarse stone cover. By contrast, the lowest depths were found in the grassy area on the northern side of the plateau, where periglacial blockfields/blockstreams are absent (ERT6 in Fig. 1a). A decrease in soil thickness was also observed close to the rock outcrops present in the plateau. Even if ERT surveys had lower vertical resolution with respect to GPR profiles, soil depth and thickness estimations from electrical resistivity gradient maxima were straightforward and provided a less subjective estimation in these complex subsurface settings.

Regarding the potential permafrost presence and distribution, relatively low electrical resistivity values pointed towards the absence of relevant bodies of permafrost in the investigated area (e.g. Kneisel, 2006), also considering the lithology of the bedrock and its fracturing conditions. This is in agreement with the BTS values, which indicated higher likelihood of permafrost presence in the southern portion of the plateau, while in the northern portion (where we performed our investigations) generally warmer values suggested only the potential presence of sporadic permafrost (cf., Julián and Chueca, 2007). Interestingly, a correspondence between a cold BTS spot and a high resistivity body was found. In this spot, we hypothesize the presence of a body of isolated permafrost, which is in agreement with its local setting. Further confirmation of the current mostly permafrost-free conditions of the area derived from the GT data, which evidenced the absence of permafrost at all depths at the borehole site and relatively warm winter temperatures.

Considering the remarkable thickness of the soil layer (particularly where periglacial features are thicker) and its general wide distribution, we assume that the overall C-stock of the plateau may be higher. In particular, the southern and south-western portions of the plateau (impossible to investigate except by means of heavy machinery) are covered by a particularly coarse and thick block cover, which resembles the eastern part where the soil thickness and C stocks are larger. In this area, like in the one overlying the high-resistivity body along the ERT3, the coarse stones thus protect soil C and permafrost conditions at depth as well.

5 Conclusion and perspectives

During the operational activities for a new chair lift construction at the Stolenberg Plateau, the opening of soil trenches revealed, unexpectedly, the presence of extremely well-developed soils under a thick stony cover consisting of periglacial blockfields and blockstreams. These soils, classified as Umbrisol, were characterized by surprisingly high C stocks, comparable to alpine tundra or even forest soils, despite the lack of vegetation and the presence of the stony cover. The application of non-invasive geophysical methods revealed that these hidden soils were widespread on the plateau under the stony cover, with a mean thickness of around 50 cm, that generally increase (up to ca. 90 cm) where the periglacial blockfields/blockstreams were thickest.

These C-rich soils, without vegetation and hidden inside periglacial landforms, may represent a unique pedoenvironment suggesting new perspective on the actual C stocks in high-elevation environment, which are probably underestimated. Since the origin of these C-rich soils inside blockstreams and blockfields is apparently in contrast with present day condition, these findings may be of great relevance for unravelling the history of the high-elevation landscape of the Monte Rosa area. For instance, if these soils represent buried paleosols below moving stone layers, they might retain information about past climate. Alternatively, in order to explain the high organic matter content below the stone cover considering recent conditions, it may be argued that decomposition rates are extremely low as a result of the cooling effect of the stone cover. To clear up those unresolved questions, a more precise characterization of the organic matter, its age and plant remains has to be performed by further studies in the area.

Acknowledgements

This study was supported by European Regional Development Fund in Interreg Alpine Space project Links4Soils (ASP399): Caring for Soil—Where Our Roots Grow. (http://www.alpinespace.eu/projects/links4soils/en/the-project). Many thanks to Monterosa Ski Resort (project stakeholder) for providing logistical support.

References

Alberto, W., Palomba, M., Perotti, L., 2018. SMART GROUND project test-sites topographic and morphologic characterization: Instruments and methodologies. Rendiconti Online Società Geologica Italiana 46, 107–114. https://doi.org/10.3301/ROL.2018.60

Allred B.J., Daniels J.J., Ehsani M.R., 2008. Handbook of Agricultural Geophysics. CRC Press Taylor Francis Group, Boca Raton. https://doi.org/10.1201/9781420019353

Andre F., van Leeuwen C., Saussez S., van Durmen R., Bogaert P., Moghadas D., de Resseguier L., Delvaux B., Vereecken H.; Lambot S., 2012. High-resolution imaging of a vineyard in south of France using ground penetrating radar, electromagnetic induction and electrical resistivity tomography. Journal of Applied Geophysics, 78, 113–122. https://doi.org/10.1016/j.jappgeo.2011.08.002

Archie, G.E., 1942. The electrical resistivity log as an aid in determining some reservoir characteristics. Trans. Am. Inst. Mech. Eng. 146, 54–67. https://doi.org/10.2118/942054-G

Arteaga, G.Á., Calderón, N.G., Krasilnikov, P.V., Sedov, S.N., Targulian, V.O., Rosas, N.V., 2008. Soil altitudinal sequence on base-poor parent material in a montane cloud forest in Sierra Juárez, Southern Mexico. Geoderma 144, 593–612. https://doi.org/10.1016/j.geoderma.2008.01.025

Ballantyne, C.K., Matthews, J.A., 1982. The development of sorted circles on recently deglaciated terrain, Jotunheimen, Norway. Arctic and Alpine Research 14, 341–354. https://doi.org/10.1080/00040851.1982.12004316

Ballantyne, C. K. (2010). A general model of autochthonous blockfield evolution. Permafrost and Periglacial Processes, 21(4), 289-300. https://doi.org/10.1002/ppp.700

Baroni, C., Orombelli, G., 1996. The Alpine "Iceman" and Holocene Climatic Change. Quat. res. 46, 78–83. https://doi.org/10.1006/qres.1996.0046

Batjes, N.H., 1996. Total carbon and nitrogen in the soils of the world. Eur J Soil Science 47, 151–163. https://doi.org/10.1111/j.1365-2389.1996.tb01386.x

Birchak, J.R., Gardner, C.G., Hipp, J.E., and Victor, J.M., 1974. High dielectric constant microwave probes for sensing soil moisture: Proc. IEEE, 62, 93-98. DOI: 10.1109/PROC.1974.9388

Biskaborn, B.K., Smith, S.L., Noetzli, J., Matthes, H., Vieira, G., Streletskiy, D.A., Schoeneich, P., Romanovsky, V.E., Lewkowicz, A.G., Abramov, A., Allard, M., Boike, J., Cable, W.L., Christiansen, H.H., Delaloye, R., Diekmann, B., Drozdov, D., Etzelmüller, B., Grosse, G., Guglielmin, M., Ingeman-Nielsen, T., Isaksen, K., Ishikawa, M., Johansson, M., Johannsson, H., Joo, A., Kaverin, D., Kholodov, A., Konstantinov, P., Kröger, T., Lambiel, C., Lanckman, J.-P., Luo, D., Malkova, G., Meiklejohn, I., Moskalenko, N., Oliva, M., Phillips, M., Ramos, M., Sannel, A.B.K., Sergeev, D., Seybold, C., Skryabin, P., Vasiliev, A., Wu, Q., Yoshikawa, K., Zheleznyak, M., Lantuit, H., 2019. Permafrost is warming at a global scale. Nat Commun 10, 264. https://doi.org/10.1038/s41467-018-08240-4

Bockheim, J.G., Munroe, J.S., 2014. Organic Carbon Pools and Genesis of Alpine Soils with Permafrost: A Review. Arctic, Antarctic, and Alpine Research 46, 987–1006. https://doi.org/10.1657/1938-4246-46.4.987

Bockheim, J.G., Tarnocai, C., 1998. Recognition of cryoturbation for classifying permafrost-affected soils. Geoderma 81, 281–293. https://doi.org/10.1016/S0016-7061(97)00115-8

Bojko, O., Kabala, C., 2017. Organic carbon pools in mountain soils — Sources of variability and predicted changes in relation to climate and land use changes. CATENA 149, 209–220. https://doi.org/10.1016/j.catena.2016.09.022

Boone R.D., Grigal D.F., Sollins P., Ahrens R.J., Armstring, D.E., 1999. Soil sampling, preparation, archiving, and quality control. In: Robertson G.P., Coleman D.C., Bledsoe C.S., Sollins P., (eds) Standard soil methods for long-termecological research. Oxford University Press, New York, pp 3–28.

Carrivick, J.L., Smith, M.W., Quincey, D.J., 2016. Structure from Motion in the Geosciences. John Wiley & Sons, Ltd, Chichester, UK. https://doi.org/10.1111/phor.12173

Celi, L., Rosso, F., Freppaz, M., Agnelli, A., Zanini, E., 2010. Soil Organic Matter Characteristics in Sporadic Permafrost-affected Environment (Creux du Van, Switzerland). Arctic, Antarctic, and Alpine Research 42, 1–8. https://doi.org/10.1657/1938-4246-42.1.1

Chiti, T., Díaz-Pinés, E., Rubio, A., 2012. Soil organic carbon stocks of conifers, broadleaf and evergreen broadleaf forests of Spain. Biology and Fertility of Soils, 48(7), 817-826. DOI 10.1007/s00374-012-0676-3

Colombo, N., Sambuelli L., Comina C., Colombero C., Giardino M., Gruber, S., Viviano, G., Vittori Antisari, L., Salerno, F., 2018. Mechanisms linking active rock glaciers and impounded surface water formation in high-mountain areas. Earth Surface Processes and Landforms, 43(2), 417-431. DOI: 10.1002/esp.4257

Colombo, N., Salerno, F., Martin, M., Malandrino, M., Giardino, M., Serra, E., Godone, D., Said-Pullicino, D., Fratianni, S., Paro, L., Tartari, G., Freppaz, M., 2019. Influence of permafrost, rock and ice glaciers on chemistry of high-elevation ponds (NW Italian Alps). Science of The Total Environment, 685, 886-901. https://doi.org/10.1016/j.scitotenv.2019.06.233

D’Amico, M., Gorra, R., Freppaz, M., 2015. Small-scale variability of soil properties and soil–vegetation relationships in patterned ground on different lithologies (NW Italian Alps). CATENA 135, 47–58. https://doi.org/10.1016/j.catena.2015.07.005

D'Amico, M.E., Pintaldi, E., Catoni, M., Freppaz, M., Bonifacio, E., 2019. Pleistocene periglacial imprinting on polygenetic soils and paleosols in the SW Italian Alps. Catena, 174, 269-284. https://doi.org/10.1016/j.catena.2018.11.019

D’Amico, M.E., Pintaldi, E., Sapino, E., Colombo, N., Quaglino, E., Stanchi, S., Navillod, E., Rocco, R., Freppaz, M., 2020. Soil Types of the Aosta Valley (NW Italy). J. Maps. https://doi.org/10.1080/17445647.2020.1821803

Daniels, D.J., 2004. Ground Penetrating Radar. 2nd edition. Radar, Sonar, Navigation and Avionics Series 15, Institute of Electrical Engineers, London, UK. DOI: 10.1049/PBRA015E

Dong, C., 1999. PowderX: Windows-95 based program for powderX-ray diffraction data processing. J Appl Crystallogr. 32, 838. https://doi.org/10.1107/S0021889899003039

Doolittle, J.A., Collins M.E., 1995. Use of soil information to determine application of ground penetrating radar. Journal of Applied Geophysics, 33, 101–108. https://doi.org/10.1016/0926-9851(95)90033-0

Egli, M., Mirabella, A., Sartori, G., Zanelli, R., and Bischof, S., 2006: Effect of north and south exposure on weathering rates and clay mineral formation in alpine soils. Catena, 67, 155–174. https://doi.org/10.1016/j.catena.2006.02.010

European Commission, 1992. Council Directive 92/43/EEC of 21 May 1992 on the conservation of natural habitats and of wild fauna and flora. Official Journal of the European Union 206, 7–50. http://data.europa.eu/eli/dir/1992/43/oj

FAO, 2006. Guidelines for soil description, 4th ed., 2006. Food and Agriculture Organization of the United Nations, Rome. ISBN 92-5-105521-1

Freppaz, M., Viglietti, D., Balestrini, R., Lonati, M., Colombo, N., 2019. Climatic and pedoclimatic factors driving C and N dynamics in soil and surface water in the alpine tundra (NW-Italian Alps). NC 34, 67–90. https://doi.org/10.3897/natureconservation.34.30737

Friedman, S.P., 2005. Soil properties influencing apparent electrical conductivity: a review. Comput. Electron. Agric. 46, 45–70. https://doi.org/10.1016/j.compag.2004.11.001

Garlato, A., Obber, S., Vinci, I., Sartori, G., Manni, G., 2009. Stock attuale di carbonio organico nei suoli di montagna del Veneto. Studi Trentini di Scienze Naturali. Suoli degli ambienti alpini 85, 69–82. ISSN 203 5-7 699

Gerdol, R., Smiraglia, C., 1990. Correlation between vegetation pattern and microtopography in periglacial areas of the Central Alps. Pirineos 135, 13–28. https://doi.org/10.3989/pirineos.1990.v135.208

Goodfellow, B. W., 2007. Relict non-glacial surfaces in formerly glaciated landscapes. Earth-Science Reviews, 80(1-2), 47-73.

Hagedorn, F., Mulder, J., Jandl, R., 2010a. Mountain soils under a changing climate and land-use. *Biogeochemistry*, *97*(1), 1-5. DOI: 10.1007/s10533-009-9386-9

Hagedorn, F., Martin, M., Rixen, C. et al., 2010b. Short-term responses of ecosystem carbon fluxes to experimental soil warming at the Swiss alpine treeline. Biogeochemistry 97, 7–19. https://doi.org/0.1007/s 10533-009-9297-9

Hoelzle, M., 1992. Permafrost occurrence from BTS measurements and climatic parameters in the Eastern Swiss Alps. Permafrost Periglac 3, 143–147. https://doi.org/10.1002/ppp.3430030212

Hoffmann, U., Hoffmann, T., Johnson, E.A., Kuhn, N.J., 2014. Assessment of variability and uncertainty of soil organic carbon in a mountainous boreal forest (Canadian Rocky Mountains, Alberta). Catena 113, 107–121. https://doi.org/10.1016/j.catena.2013.09.009

Islam A.K.M.E., Lotse, E.G., 1986. Quantitative mineralogical analysis of some Bangladesh soils with X-ray, ion exchange and selective dissolution techniques. Clay Miner. 21, 31–42. https://doi.org/10.1180/claymin.1986.021.1.03

IUSS Working Group WRB, 2015. World Reference Base for Soil Resources 2014, update 2015. International soil classification system for naming soils and creating legends for soil maps. World Soil Resources Reports No. 106. FAO, Rome. E-ISBN 978-92-5-108370-3

Julián, A., Chueca, J., 2007. Permafrost distribution from BTS measurements (Sierra de Telera, central Pyrenees, Spain): assessing the importance of solar radiation in a mid-elevation shaded mountainous area. Permafrost Periglac 18, 137–149. https://doi.org/10.1002/ppp.576

Karte, J., 1983. Periglacial phenomena and their significance as climatic and edaphic indicators. *GeoJournal*, *7*(4), 329-340. https://doi-org.bibliopass.unito.it/10.1007/BF00241455

Kneisel, C., 2006. Assessment of subsurface lithology in mountain environments using 2D resistivity imaging. *Geomorphology*, *80*(1-2), 32-44. https://doi.org/10.1016/j.geomorph.2005.09.012

Kneisel, C., Hauck, C., Fortier, R. and Moorman, B., 2008. Advances in geophysical methods for permafrost investigations. Permafrost Periglac. Process., 19: 157-178. doi:10.1002/ppp.616

Knowles, J.F., Blanken, P.D., Lawrence, C.R., Williams, M.W., 2019. Evidence for non-steady-state carbon emissions from snow-scoured alpine tundra. Nat Commun 10, 1306. https://doi.org/10.1038/s41467-019-09149-2.

Léger, E., Dafflon B., Soom, F., Peterson J., Ulrich C., Hubbard, S., 2017. Quantification of Arctic Soil and Permafrost Properties Using Ground-Penetrating Radar and Electrical Resistivity Tomography Datasets, in IEEE Journal of Selected Topics in Applied Earth Observations and Remote Sensing, vol. 10, no. 10, pp. 4348-4359. doi: 10.1109/JSTARS.2017.2694447

Leifeld, J., Zimmermann, M., Fuhrer, J., Conen, F., 2009. Storage and turnover of carbon in grassland soils along an elevation gradient in the Swiss Alps. Global Change Biology 15, 668–679. https://doi.org/10.1111/j.1365-2486.2008.01782.x

Leopold, M., Voelkel, J., Dethier, D., Williams, M., & Caine, N., 2010. Mountain permafrost—a valid archive to study climate change? Examples from the Rocky Mountains Front Range of Colorado, USA. Nova Acta Leopoldina, 112(384), 281-289.

Magnani, A., Viglietti, D., Godone, D., Williams, M.W., Balestrini, R., Freppaz, M., 2017. Interannual Variability of Soil N and C Forms in Response to Snow—Cover duration and Pedoclimatic Conditions in Alpine Tundra, Northwest Italy. Arctic, Antarctic, and Alpine Research 49, 227–242. https://doi.org/10.1657/AAAR0016-037

Mattirolo, E., Novarese, V., Franchi, S., Stella, A., 1951. Carta Geologica D'Italia 1:100000, foglio 29. Istituto Geografico Militare. Firenze, Italy

McClymont, A. F., Hayashi, M., Bentley, L. R., Muir, D., Ernst, E., 2010. Groundwater flow and storage within an alpine meadow-talus complex, Hydrol. Earth Syst. Sci., 14, 859–872, https://doi.org/10.5194/hess-14-859-2010.

Mollaret, C., Hilbich, C., Pellet, C., Flores-Orozco, A., Delaloye, R., Hauck, C., 2019. Mountain permafrost degradation documented through a network of permanent electrical resistivity tomography sites. The Cryosphere 13, 2557–2578. https://doi.org/10.5194/tc-13-2557-2019

Moorman, B. J., Robinson, S., Burgess, M. M., 2003. Imaging periglacial conditions with ground-penetrating radar. Permafrost and Periglacial Processes 14 (4), 319-329. https://doi.org/10.1002/ppp.463

Novàkovà, E., Karous, M., Zajiček, A., Karousovà, M., 2013. Evaluation of ground penetrating radar and vertical electrical sounding methods to determine soil horizons and bedrock at the locality Dehtáře. Soil & Water Res., 8 (3), pp. 105-112. https://doi.org/10.17221/6/2012-SWR

Otto, J.C., Sass, O., 2006. Comparing geophysical methods for talus slope investigations in the Turtmann valley (Swiss Alps), Geomorphology, Volume 76, Issues 3–4, 257-272. https://doi.org/10.1016/j.geomorph.2005.11.008.

Pellet, C., Hilbich, C., Marmy, A., & Hauck, C., 2016. Soil moisture data for the validation of permafrost models using direct and indirect measurement approaches at three alpine sites. Frontiers in Earth Science, 3, 91. https://doi.org/10.3389/feart.2015.00091

Samouelian, A., Cousin, I., Tabbagh, A., Bruand, A., Richard, G., 2005. Electrical resistivity survey in soil science: A review, Soil Tillage Res., 83, 173–193, doi:10.1016/j.still.2004.10.004.

Schuur, E.A.G., Abbott, B.W., Bowden, W.B., Brovkin, V., Camill, P., Canadell, J.G., Chanton, J.P., Chapin, F.S., Christensen, T.R., Ciais, P., Crosby, B.T., Czimczik, C.I., Grosse, G., Harden, J., Hayes, D.J., Hugelius, G., Jastrow, J.D., Jones, J.B., Kleinen, T., Koven, C.D., Krinner, G., Kuhry, P., Lawrence, D.M., McGuire, A.D., Natali, S.M., O'Donnell, J.A., Ping, C.L., Riley, W.J., Rinke, A., Romanovsky, V.E., Sannel, A.B.K., Schädel, C., Schaefer, K., Sky, J., Subin, Z.M., Tarnocai, C., Turetsky, M.R., Waldrop, M.P., Walter Anthony, K.M., Wickland, K.P., Wilson, C.J., Zimov, S.A., 2013. Expert assessment of vulnerability of permafrost carbon to climate change. Climatic Change 119, 359–374. https://doi.org/10.1007/s10584-013-0730-7

Smith, M.V., Carrivick J.L., Quincey D.J., 2015. Structure from motion photogrammetry. Physical Geography 40, 247–275. https://doi.org/10.1177/0309133315615805

Stanchi, S., Freppaz, M., Walter, S., & Vanderwegen, L., 2015. Mountain soils and threats. In Understanding Mountain Soils: A Contribution from Mountain Areas to the International Year of Soils 2015; Romeo, R., Vita, A., Manuelli, S., Zanini, E., Freppaz, M., Stanchi, S., Eds.; FAO: Rome, Italy, 2015; pp. 88–90, ISBN 978-92-5-108804-3.

Van Reeuwijk, L.P., 2002. Procedures for Soil Analysis. Technical Paper n. 9. ISBN: 90-6672-044-1

Van Vliet-Lanoë, B., 2014. Patterned ground and climate Change. In: Podrovsky, O. (Ed.), Permafrost: Distribution, Composition and Impacts on Infrastructure and Ecosystems. Nova Science Publishers, Inc. chap 2 pp.67–106. (Results of the IPEV CRYOCLIM 2004 program).

Wharton, R.P., Hazen, G.A., Rau, R.A., Best, D.L., 1980. Electromagnetic propagation logging--advances in technique and interpretation: Soc. Petr. Eng., 55th Annual Technical Conference, Paper 9267.

Wilson, P., 2013. Block/Rock streams. In Encyclopedia of Quaternary Science, S.A. Elias, Ed., 3. Elsevier: Amsterdam; 514–522. DOI: 10.1016/B978-0-444-53643-3.00102-3

Zollinger, B., Alewell, C., Kneisel, C., Meusburger, K., Gärtner, H., Brandová, D., Ivy-Ochs, S., Schmidt, M.W.I., Egli, M., 2013. Effect of permafrost on the formation of soil organic carbon pools and their physical–chemical properties in the Eastern Swiss Alps. CATENA 110, 70–85. https://doi.org/10.1016/j.catena.2013.06.010

Figures

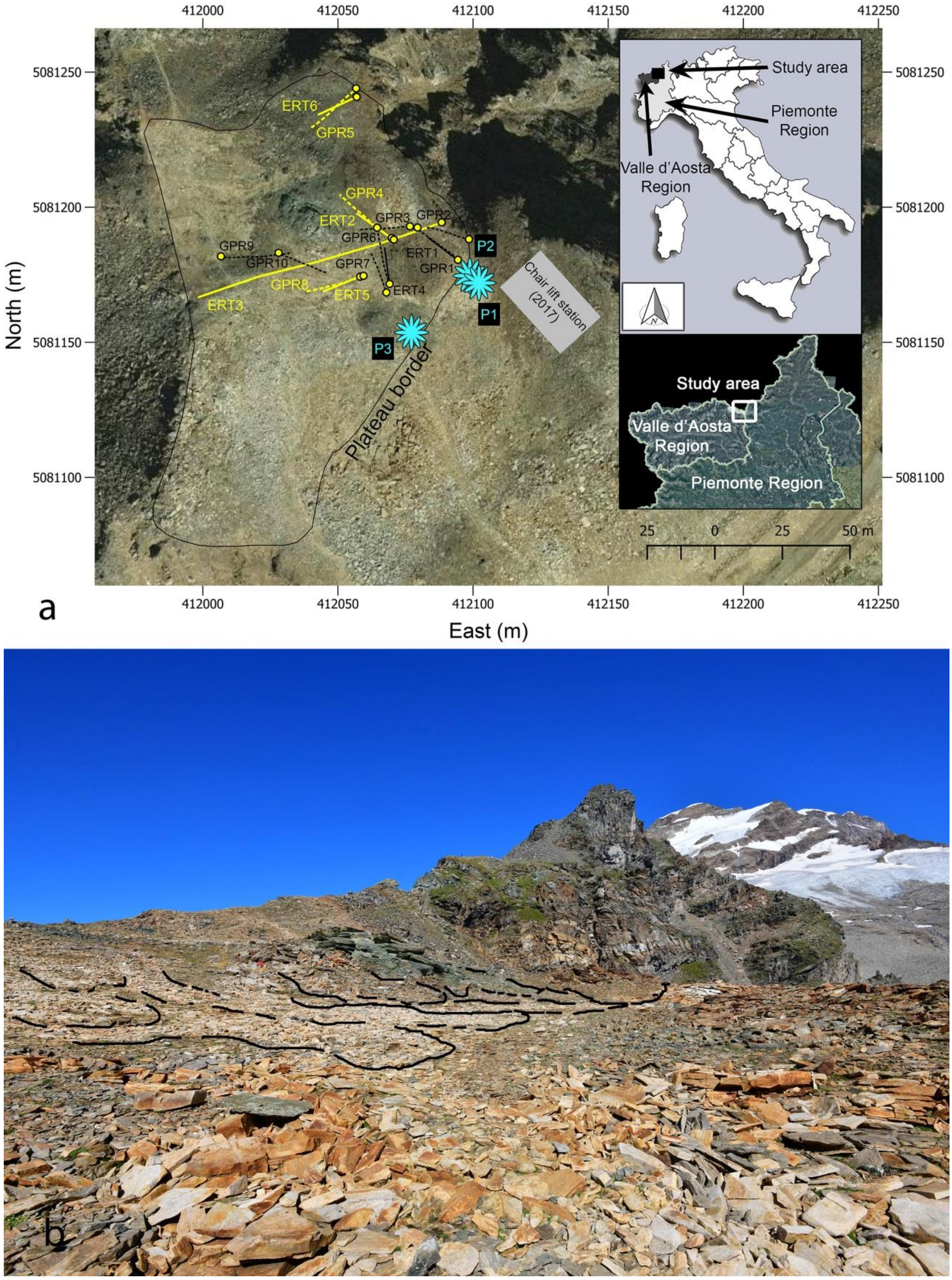

Figure 1. (a) Location of the study area in the NW Italian Alps (www.pcn.minambiente.it), and overview of the study area (orthoimage Piemonte Region, year 2010); solid and dashed lines indicate ERT and GPR profiles, respectively. Yellow lines indicate the profiles showed and discussed in the manuscript. Yellow circles identify the starting point of each geophysical profile. Cyan polygons indicate the location of the three soil profiles (P1, P2, and P3). (b) View of the plateau (photo by M. D'Amico); dashed lines indicate blockstreams.

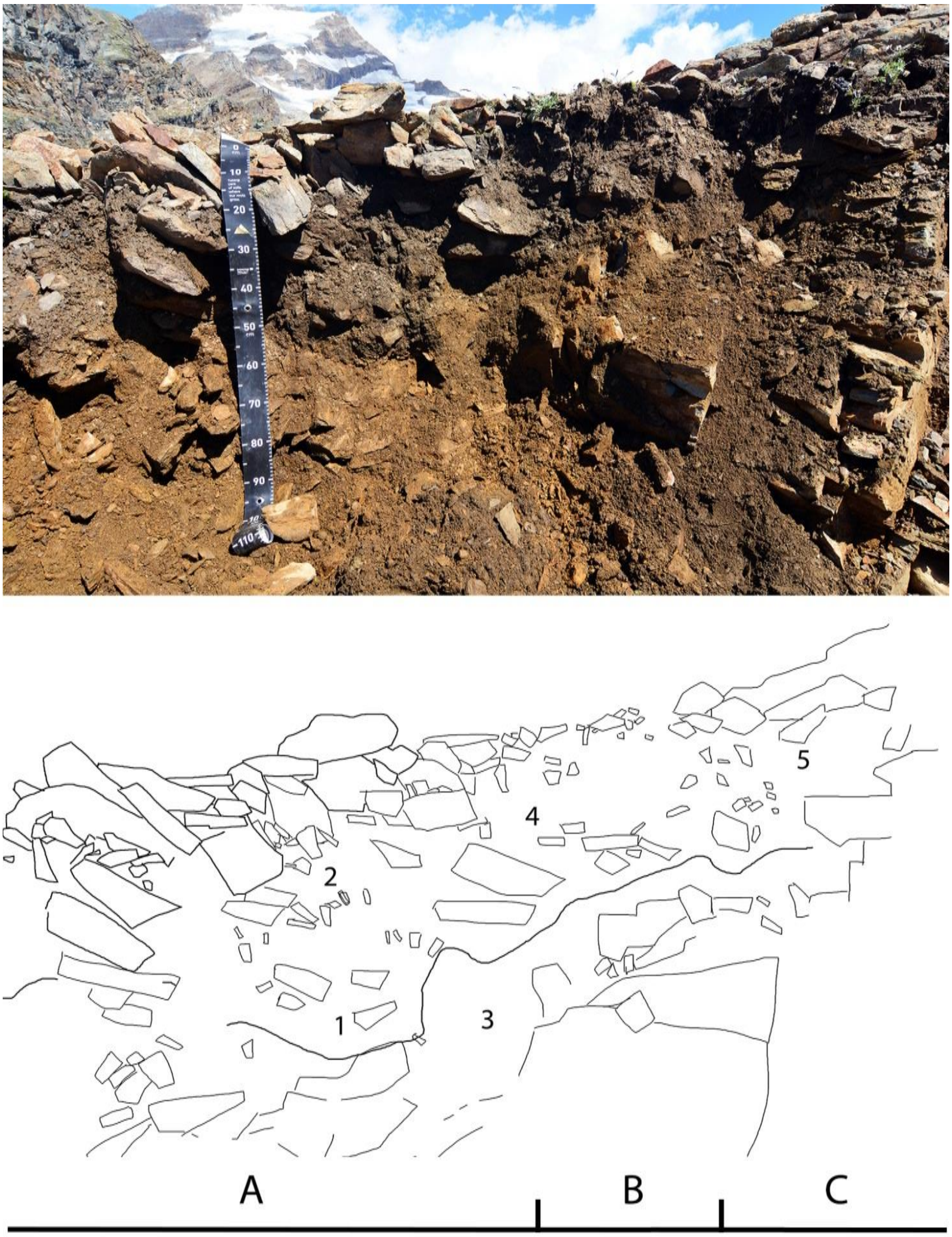

Figure 2. Soil profile P1, with the corresponding scheme (below) reporting sampling points (number), the horizon limits (lines therein) and sectors (letters) in which C-stocks were estimated.

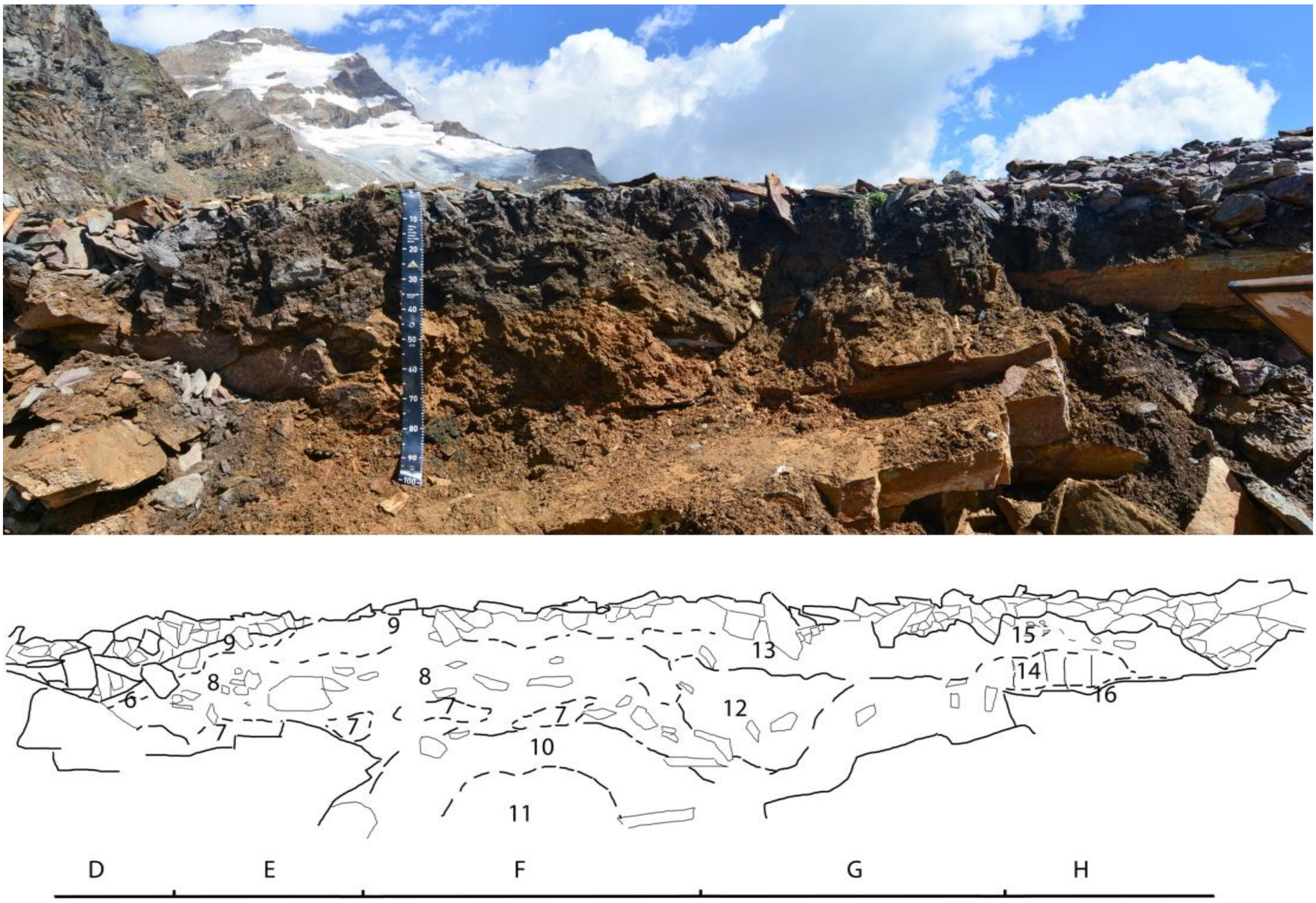

Figure 3. Soil profile P2, with the corresponding scheme (below) reporting sampling points (number), the horizon limits (lines therein) and sectors (letters) in which C-stocks were estimated.

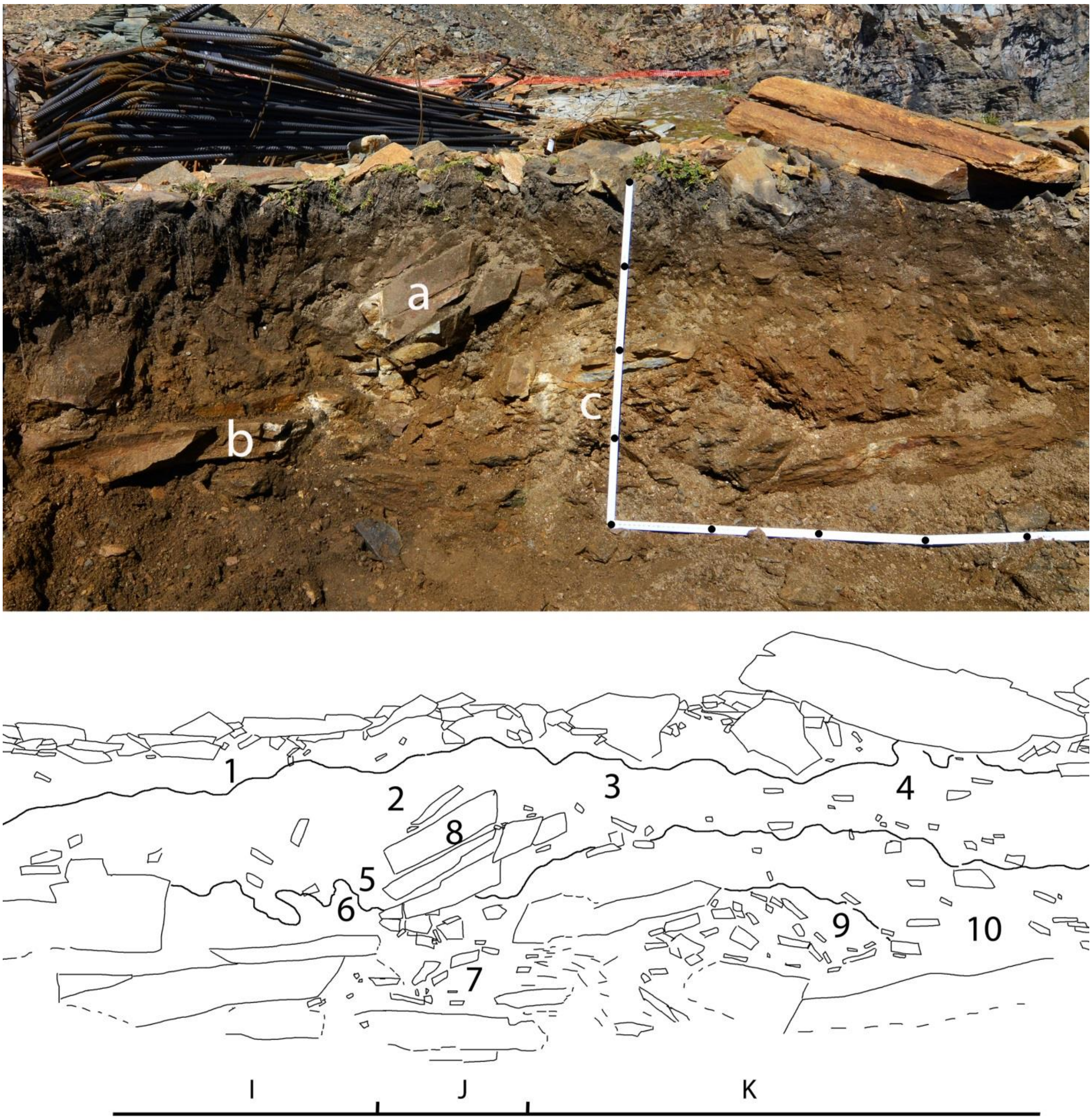

Figure 4. Soil profile P3, with the corresponding scheme (below) reporting sampling points (number), the horizon limits (lines therein) and sectors (letters I, J, K) in which C-stocks were estimated. Letter "a" indicates blocks dislocated from the rock layer evidenced by letters "b" and "c", above a deep fracture (wedge); notches in the meter rule indicate 20 cm intervals.

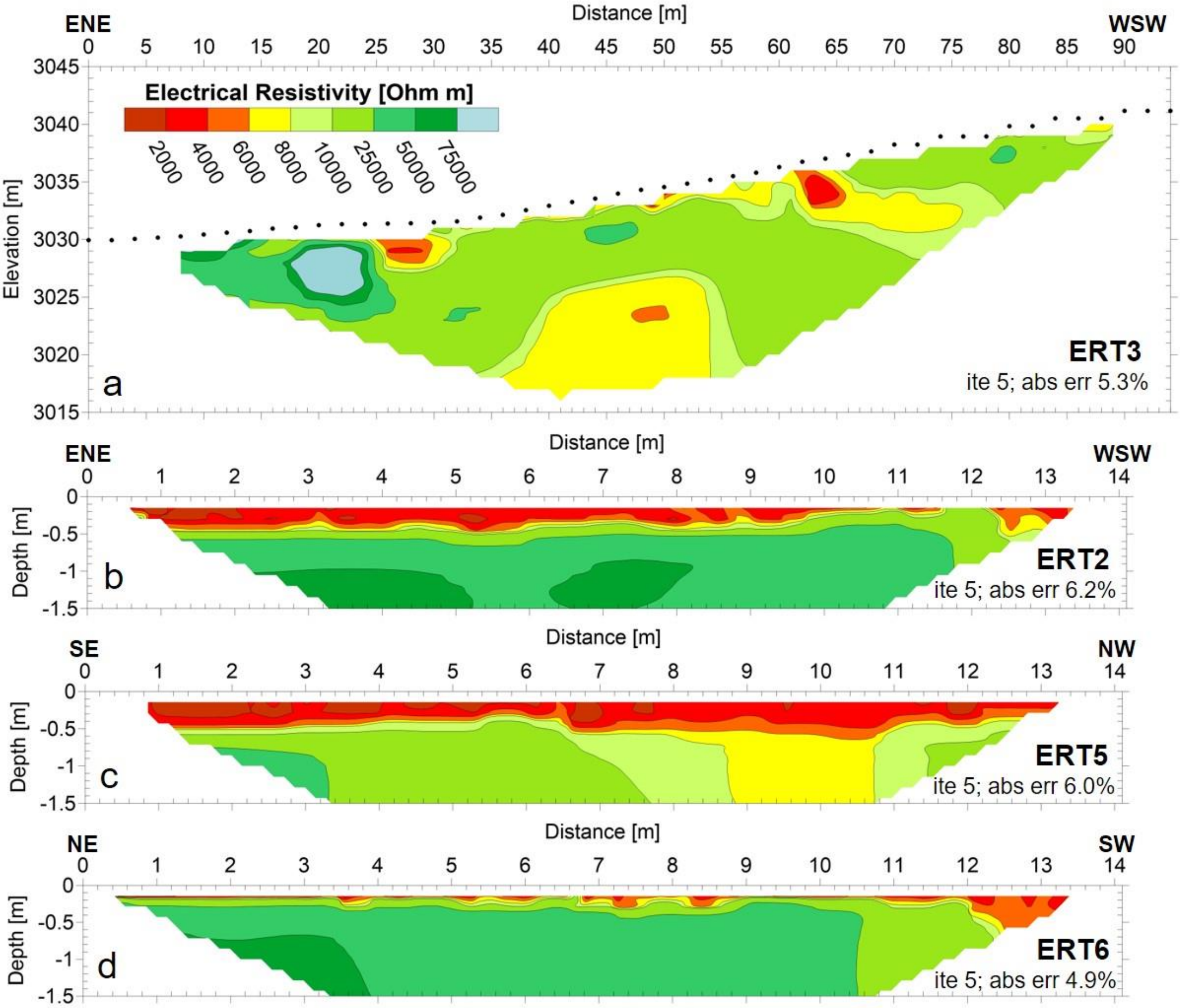

629

630 **Figure 5. ERT sections: (a) ERT3 (long); (b) ERT2; (c) ERT5; (d) ERT6. The location of the ERT lines is reported in Figure 1. Short**
631 **sections are cut at 1.5-m depth.**

632

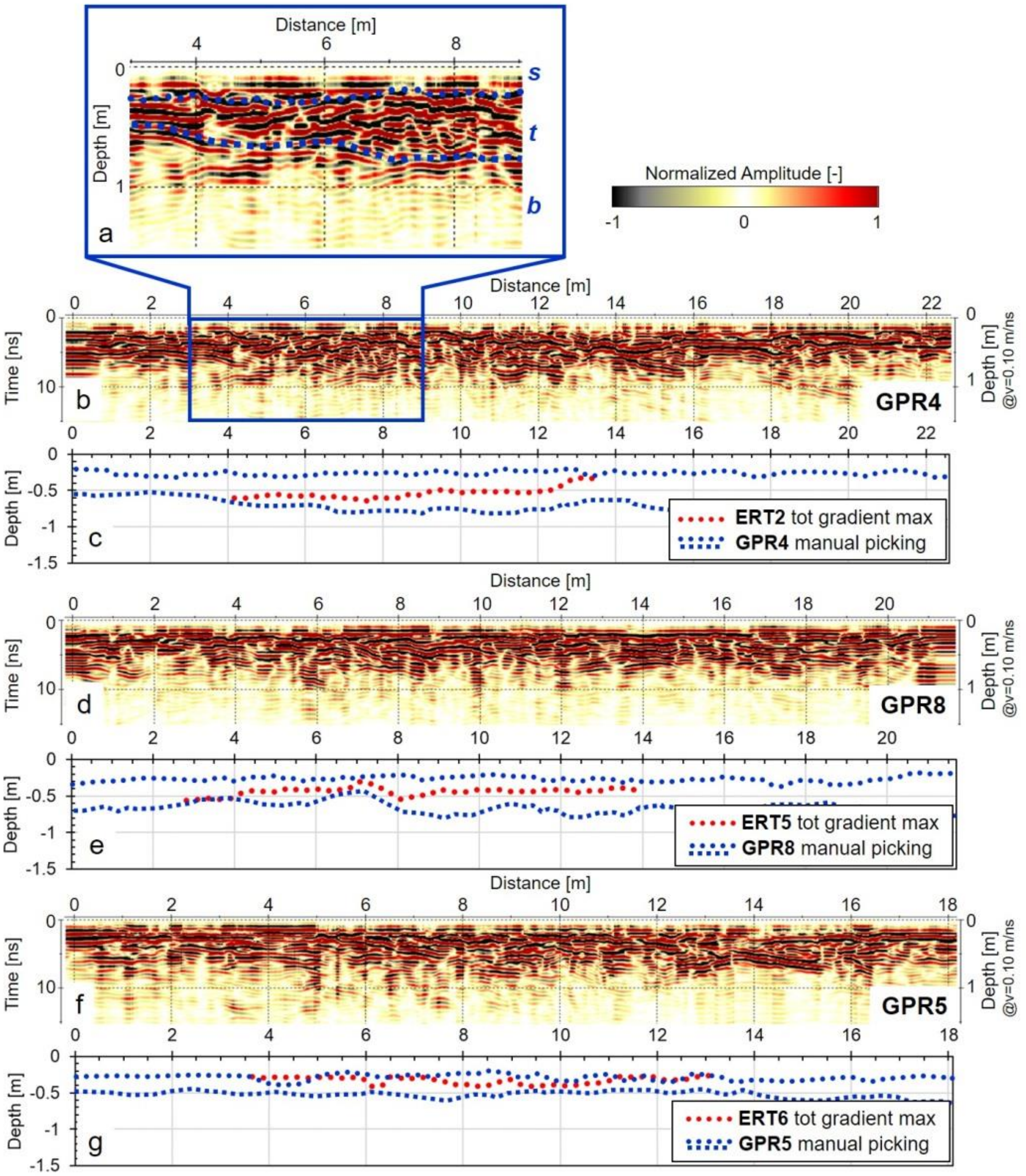

Figure 6. GPR sections. (a) Zoom on GPR4 section with tentative interpretation of the shallow stratigraphy: soil (s), soil-to-bedrock transition (t), bedrock (b). (b, d, f) Processed radargrams for lines GPR4, GPR8, GPR5 (vertical cut at 1.5-m depth). (c, e, g) Soil bottom estimation on the above sections. Comparison between the location of the electrical resistivity gradient maxima computed on the ERT lines of Figure 5 (red dots) and the piking of the different layers on GPR results as shown in Figure 6a (in blue, dotted line: s-t interface, dashed line t-b interface). The location of the GPR profiles is reported in Figure 1.

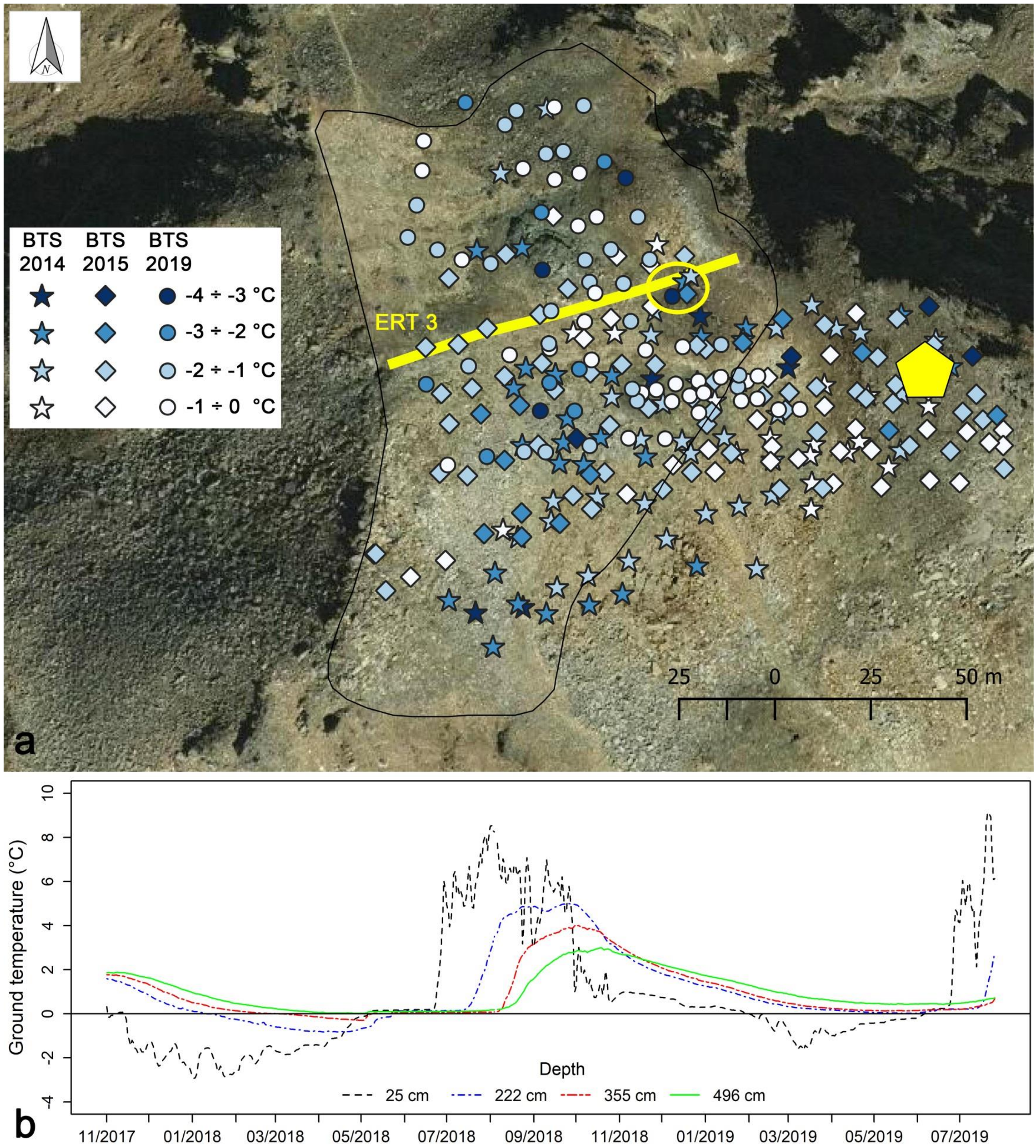

Figure 7. (a) Location and bottom temperatures of the snow cover (BTS) measurements in 2014, 2015, and 2019. Yellow line represents the ERT3; yellow oval indicates the area of correspondence between a cold spot and the high resistivity body detected by the ERT3; yellow polygon indicates the borehole location for the measurement of ground temperature (GT). (b) GT values measured in the 5-m deep borehole of the station managed by Arpa Piemonte in the northern side of the plateau.

Tables

Sample number	Horizon	Munsel colour, moist	Stone fragments (%)	Clay (%)	Silt (%)	Sand (%)	Textural class	Structure	pH	TOC (%)	TN (%)	TOC/TN	BD (kg m^{-3})	TH (m)	VF	C-STOCK (kg m^{-2})
P1																
1	A2	10YR 3/2	30	2.8	14.5	82.7	LS	SB	4.8	1.90	0.10	20	1000	0.20	0.70	2.66
2	A1	10YR 3/2	30	2.5	14.9	82.5	LS	SB	4.4	1.08	0.08	13	1000	0.30	0.70	2.26
3	BA	10YR 3/3	40	1.6	23.3	75.2	LS	BL	4.8	0.47	0.04	11	1200	0.20	0.60	0.68
4	A1+A2	10YR 3/2	40	2.7	15.3	82.0	LS	GR	4.7	1.20	0.10	11	1000	0.30	0.60	2.17
5	A	10YR 3/2	80	2.7	14.5	82.9	LS	GR	4.4	1.86	0.15	13	1000	0.20	0.20	0.74
P2																
6	A	10YR 2/1	30	2.6	20.8	76.5	LS	SB	4.3	0.80	0.08	11	1000	0.20	0.70	1.12
7	A@	10YR 3/2	10	2.3	23.2	74.5	LS	PL/SB	5.6	2.05	0.11	19	1100	0.05	0.90	1.02
8	A2	10YR 3/3	30	1.9	18.3	79.8	LS	SB	4.7	1.10	0.08	14	1000	0.20	0.70	1.53
9	A1	10YR 3/2	70	2.5	12.1	85.4	LS	GR	4.4	1.13	0.11	11	1000	0.10	0.30	0.34
10	BC	10YR 4/4	70	1.4	27.6	71.0	SL	PL/SB	5.3	0.14	BDL	-	1200	0.20	0.30	0.10
11	CB	10YR 5/2	70	1.0	26.3	72.7	LS	SB	5.9	BDL	BDL	-	1200	0.20	0.30	0.00
12	BW	10YR 3/4	60	0.9	25.7	73.4	LS	SB	5.2	0.26	0.03	9	1200	0.20	0.40	0.25
13	A	10YR 3/2	30	4.3	24.1	71.6	SL	BL	4.8	1.09	0.08	14	1000	0.15	0.70	1.15
14	BA	10YR 3/3	50	2.8	29.3	67.9	SL	CO/PR	4.9	1.10	0.07	15	1200	0.20	0.50	1.32
15	A	10YR 3/2	10	3.9	14.0	82.1	LS	GR	4.5	0.71	0.09	8	1000	0.15	0.90	0.96
16	Silt caps	10YR 6/4	10	6.2	41.9	51.9	SL	PL	5.0	0.28	0.03	8	1300	0.03	0.90	0.10
P3																
1	A1	10YR 2/1	70	4.3	8.0	87.7	S	GR	4.9	0.56	0.05	12	1000	0.05	0.30	0.08
2	A2	10YR 3/2	5	3.2	15.6	81.2	LS	GR	4.9	0.87	0.05	17	1000	0.28	0.95	2.28
3	A2	10YR 3/2	5	4.2	15.6	80.1	LS	CO	4.9	1.05	0.07	15	1000	0.25	0.95	2.49
4	A2	10YR 3/2	20	4.8	28.2	66.9	SL	CO	4.8	0.76	0.05	14	1000	0.25	0.80	1.51
5	A2	10YR 3/2	0	4.8	20.7	74.4	SL	SG	4.7	1.18	0.07	17	1000	0.05	1.00	0.59
6	Bw	10YR 5/4	20	2.6	31.8	65.5	SL	SB	5.0	0.15	0.02	7	1200	0.25	0.80	0.35

7	BC	10YR 4/3	50	3.4	16.8	79.9	LS	SB	5.2	0.24	0.02	10	1200	0.20	0.50	0.29
8	A2	10YR 3/2	0	2.8	13.7	83.5	LS	GR	4.9	0.81	0.05	17	1000	0.02	1.00	0.16
9	BC	10YR 4/3	70	4.6	19.5	75.9	LS	PL	5.1	0.31	0.03	9	1200	0.20	0.30	0.22
10	Bw	10YR 3/4	40	3.3	19.6	77.1	LS	SB	5.2	0.16	0.02	8	1200	0.30	0.60	0.36

Table 1. Morphological, physical and chemical properties of the soil samples. Textural class: LS=loamy sand; SL=sandy loam. Structure: SB=subangular blocky; BL=blocky; GR=granular; PL=platy; CO=columnar; PR=prismatic; SG=single grain. BDL=below detection limit.

P1			
Sector	**Horizon**	**Sample number**	**C-STOCK$_{tot}$ (kg m^{-2})**
A	A1	2	5.18
	A2	1	
	BA	3b	
B	A1+A2	4	2.85
	BA	3	
C	A	5	0.74
P2			
D	A	6	1.12
E	A1	9	2.89
	A2	8	
	A@	7	
F	A1	9	2.99
	A2	8	
	A@	7	
	BC	10	
	CB	11	
G	A	13	1.50
	Bw	12	
	BC	10b	
H	A	15	2.38
	BA	14	
	Silt caps	16	
P3			
I	A1	1	3.30
	A2	2	
	A2	5	
	Bw	6	
J	A1	1	3.02
	A2	3	
	A2	8	
	BC	7	
K	A1	1	2.17
	A2	4	
	Bw	10	
	BC	9	

Table 2. Total C-stock of the profiles for each sector.